ACS Photonics

pubs.acs.org/journal/apchd5

Article

Frequency Manipulations in Single-Photon Quantum Transport under Ultrastrong Driving

Han Xiao,[§] Luojia Wang,[§] Luqi Yuan,[*] and Xianfeng Chen

Cite This: *ACS Photonics* 2020, 7, 2010–2017

Read Online

ACCESS | Metrics & More | Article Recommendations

ABSTRACT: All-optical manipulation of a single-photon quantum transport is of fundamental importance in quantum nanophotonics. Here, a system consisting of a single-mode waveguide coupling with a V-type three-level atom is proposed, where two excited states of the atom are strongly driven by the external coherent field. Transmission and reflection spectra for the output photon at different frequency components, including virtual transitions induced by the ultrastrong driving, are calculated. The interaction between the waveguide photon and the driven atom experiences quantum interferences, which leads to a variety of capabilities for manipulating the single-photon transport in the spectral domain. We perform simulations to demonstrate the possibilities of achieving desired frequency conversions as well as generating different correlated single-photon states by using external drive field at chosen strength. Our work therefore studies the single-photon transport in a strongly driven atom−waveguide system and shows applications for all-optically manipulating the single photon in the field of quantum information processing.

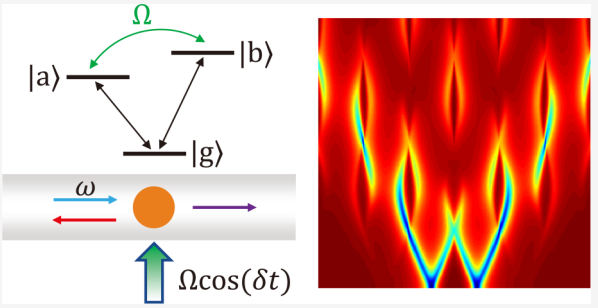

KEYWORDS: *atom−waveguide system, single-photon transport, ultrastrong driving, frequency conversion, correlated single-photon state*

With recent developments of the state-of-art quantum technology, manipulations of the single-photon quantum state transport receive great attentions, which shows an important role toward potential applications in the quantum information processing.[1−10] In an atom−waveguide system, photon confined inside the waveguide shows the strong interaction with the atom (or the quantum emitter), which provides the possibility for realizing the photon−photon interaction.[11] Many experiments have been conducted to realize different practical platforms, such as the microwave transmission line coupled to the superconducting qubit,[12,13] surface plasmons coupled to the individual optical emitter,[14] and the photonic-crystal or nanophotonic waveguide coupled to a real atom or a quantum emitter.[15−20] It has been found that the single-photon transport dynamics in such systems can be successfully studied by general approaches using real-space model Hamiltonian[21,22] and few-photon input−output formalism.[23,24] These theoretical methods therefore have been widely utilized to not only explain relevant experiments, but also to solve many specific models and predict interesting phenomena for the few-photon transport, including electromagnetically induced transparency,[25−27] slow/fast propagation of photons,[28] and stimulated emission,[29] which hence triggers a broad interest in the quantum optics community.[30−41]

Due to the strong interaction between photons and atoms inside the waveguide, the atom−waveguide systems provide a potential candidate for exploring the quantum nonlinear optics and realizing strong photon−photon interactions.[5] All-optical quantum manipulation of photons therefore is feasible, where single-photon transport can be controlled by other driven optical fields.[42−46] These methods therefore points out a possible route toward various quantum nanophotonic applications including single-photon transistor,[14] quantum phase switch,[47] single-photon router,[48,49] and entangled state manipulation.[50,51]

In this paper, we investigate the interaction between a single-photon and a V-type three-level atom (or quantum emitter) in a generalized single-mode waveguide, where the transition between two upper levels is driven by an external coherent microwave field. The photon is near resonant with both transitions corresponding to two arms of the V-type atom, and hence there are two possible paths to excite the atom from the ground state to either the excited state. With driving the two excited states by a strong external field breaking the rotating-wave approximation (RWA), the system exhibits the quantum interference characteristics with multiple paths including virtual transitions, which leads to more rich physics compared to the similar system under RWA.[42] We analyze trans-

Received: February 19, 2020
Published: July 8, 2020

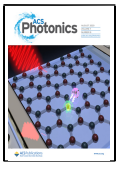

https://dx.doi.org/10.1021/acsphotonics.0c00263
ACS Photonics 2020, 7, 2010–2017

missions and reflections by using general formalisms[21−24] together with Floquet theory.[52−54] Our study explores the frequency conversion in the single-photon transport process at its most basic level and shows the feasibility for preparing frequency-correlated quantum states, which opens an avenue in the field of quantum nanophotonics toward the all-optical manipulation of a single photon in the spectral domain.

MODEL

We consider the atom-waveguide system which is composed by a single-mode waveguide coupling with a V-type three-level atom (see Figure 1a). The ground state and two excited states

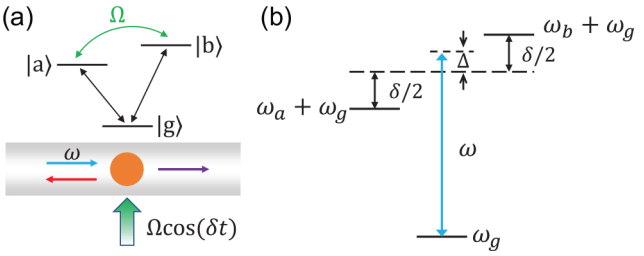

Figure 1. (a) Schematics of a single photon interacting with an atom driven by the external field inside the waveguide. A three-level atom experiences photon absorption and then releases a transmitted (purple arrow) or reflected (red arrow) photon. (b) Detailed energy levels of the V-type atom interacting with the incident photon at the frequency ω.

of the atom are described as $|g\rangle$, $|a\rangle$, and $|b\rangle$, respectively. The atom has two optical transitions $|g\rangle \rightarrow |a\rangle$ and $|g\rangle \rightarrow |b\rangle$ with the corresponding transition frequencies ω_a and ω_b, which is assumed to obey $\omega_a < \omega_b$. The incident photon inside the waveguide having a frequency ω in the vicinity of these two atomic transitions, which can excite the atom from its ground state to either excited state. In addition, external coherent driving field is used to provide an atomic transition between two excited states. This extra driving field is general and can be either microwave[55] or an effective field from a two-photon transition[56] for a given special platform. The photon−atom interaction inside the waveguide can be described by the real-space Hamiltonian[21,42]

$$H = \int \mathrm{d}x \Big\{ -iv_g C_R^\dagger(x)\frac{\partial}{\partial x}C_R(x) + iv_g C_L^\dagger(x)\frac{\partial}{\partial x}C_L(x) + V\delta(x)[(C_R^\dagger(x) + C_L^\dagger(x))(\sigma_{1,-} + \sigma_{2,-}) + \mathrm{H.c.}]\Big\} + (\omega_a + \omega_g)|a\rangle\langle a| + (\omega_b + \omega_g)|b\rangle\langle b| + \omega_g|g\rangle\langle g| + 2\Omega\cos(\delta t)(|a\rangle\langle b| + |b\rangle\langle a|) \quad (1)$$

where $\sigma_{1,-} = |g\rangle\langle a|$ and $\sigma_{2,-} = |g\rangle\langle b|$ are ladder operators giving the atomic transition from the ground state $|g\rangle$ to the excited state $|a\rangle$ and $|b\rangle$, respectively. $C_{R(L)}^\dagger$ and $C_{R(L)}$ are the creation and annihilation operators for creating and annihilating the photon propagating toward the right (left), respectively. We also set $\hbar = 1$ and $\omega_g = 0$ for the simplicity throughout this paper. We assume the linear dispersion of the waveguide and hence v_g denotes the group velocity of photon and V denotes the photon−atom coupling strength. The driving field is continuous-wave and has the oscillating frequency $\delta = \omega_b - \omega_a$, which is equal to the atomic transition between two excited states, as shown in Figure 1b. Ω is the corresponding Rabi frequency for the driving field. In deriving eq 1, we use RWA for the interaction between the waveguide photon and the atom, but we do not apply RWA for the interaction between the driving field and the atom, because we assume that the microwave transition frequency is much smaller than the optical transition frequency and the Rabi frequency of the driving field can be at the same order of the magnitude as the microwave transition frequency, that is, $\Omega \sim \omega_b - \omega_a \ll \omega_a, \omega_b$. Our model, hence, is close to the experimental condition and can be used to explore the physics from the strong external driving in the atom−waveguide system.

With the conservation of the excitation number for the single-photon transport in the waveguide, we consider the wave function of the system

$$|E(t)\rangle = \int \mathrm{d}x\{\phi_R^\dagger(x,t)C_R^\dagger(x) + \phi_L^\dagger(x,t)C_L^\dagger(x)\}|0,g\rangle + e_1(t)|0,a\rangle + e_2(t)|0,b\rangle \quad (2)$$

where $\phi_R^\dagger(x,t)$ ($\phi_L^\dagger(x,t)$) is the wave function for photon propagating along the right (left) direction, while the atom is in the ground state. $e_1(t)$ and $e_2(t)$ are probability amplitudes of the atom in excited states $|a\rangle$ and $|b\rangle$, respectively. The wave function in eq 2 satisfies the Schrödinger equation $H|E\rangle = i\frac{\partial}{\partial t}|E\rangle$. For the photon incident from the left, one can take forms

$$\phi_R^\dagger(x,t) = [e^{ikx}\theta(-x) + t(t)e^{ikx}\theta(x)]e^{-i\omega t} \quad (3)$$

$$\phi_L^\dagger(x,t) = [r(t)e^{-ikx}\theta(-x)]e^{-i\omega t} \quad (4)$$

where $t(t)$ and $r(t)$ are the transmission and reflection amplitude, respectively. k and ω is the wavevector and frequency of the incoming photon, respectively, which obeys the quality $\omega = v_g k$.

To solve the Schrödinger equation, we use the Floquet theory[52−54] since the Hamiltonian in eq 2 is periodic in time and satisfies $H(t) = H(t + 2\pi/\delta)$. Hence, one can expand the time-dependent $t(t)$, $r(t)$, and $e_{1(2)}(t)$ as

$$t(t) = \sum_n t^{(n)}e^{-in\delta t} \quad (5)$$

$$r(t) = \sum_n r^{(n)}e^{-in\delta t} \quad (6)$$

$$e_{1(2)}(t) = e^{-i\omega t}\sum_n e_{1(2)}^{(n)}e^{-in\delta t} \quad (7)$$

where $t^{(n)}$, $r^{(n)}$, and $e_{1(2)}^{(n)}$ are the corresponding terms for the components at the frequency $\omega_n = \omega + n\delta$, respectively, with n being an integer. Plugging the expressions in eqs 5−7 into the Schrödinger equation and using the slowly varying-envelope approximations, that is, $|\dot{t}|, |\dot{r}| \ll \omega|t|, \omega|r|$, we obtain

$$\left[\Delta + \left(n + \frac{1}{2}\right)\delta + i\frac{V^2}{v_g}\right]e_1^{(n)} + i\frac{V^2}{v_g}e_2^{(n)} - \Omega(e_2^{(n-1)} + e_2^{(n+1)}) = V\delta_{n,0} \quad (8)$$

$$\left[\Delta + \left(n - \frac{1}{2}\right)\delta + i\frac{V^2}{v_g}\right]e_2^{(n)} + i\frac{V^2}{v_g}e_1^{(n)} - \Omega(e_1^{(n-1)} + e_1^{(n+1)}) = V\delta_{n,0} \quad (9)$$

$$r^{(n)} = -i\frac{V}{v_g}(e_1^{(n)} + e_2^{(n)}) \quad (10)$$

$$t^{(n)} = r^{(n)} + \delta_{n,0} \quad (11)$$

https://dx.doi.org/10.1021/acsphotonics.0c00263
ACS Photonics 2020, 7, 2010−2017

where $\Delta = \omega - (\omega_a + \delta/2)$ denotes the frequency detuning of the incident photon referring to the frequency $(\omega_a + \omega_b)/2$ (see Figure 1b).

RESULTS

We solve eqs 8−11 to explore the single-photon transport in the system shown in Figure 1a. $|t^{(n)}|^2$ and $|r^{(n)}|^2$ denote the transmission probability and reflection probability for the photon being converted to the nth frequency component ω_n. Such set of equations is composed of infinite number of equations, which can be calculated with a truncation. We choose the frequency difference between two excited states $\delta = 10\ V^2/v_g$ and truncate the equations at $n = \pm 10$. In Figure 2,

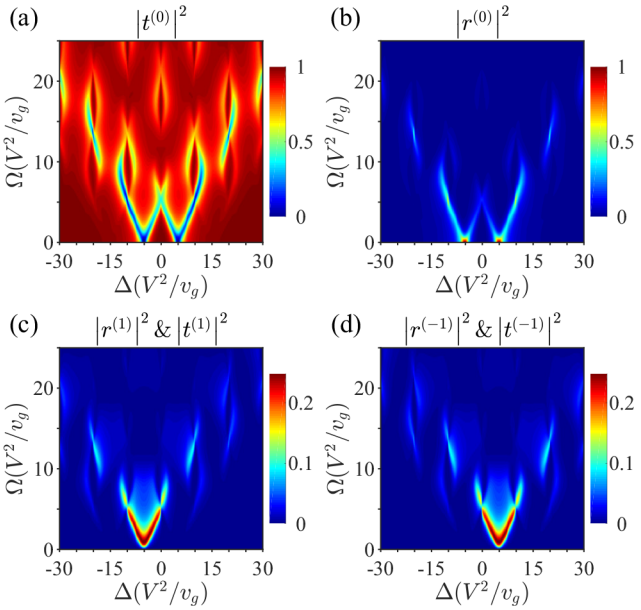

Figure 2. Transmission and reflection spectra of the single-photon transport in the atom-waveguide system with $\delta = 10\ V^2/v_g$. (a, b) Transmission and reflection spectra $|t^{(0)}|^2$ and $|r^{(0)}|^2$ for the output photon with the unchanged frequency. (c, d) Transmission and reflection spectra $|t^{(\pm1)}|^2$ and $|r^{(\pm1)}|^2$ for the output photon at the frequency $\omega_{\pm1} = \omega \pm \delta$.

we plot the transmission and reflection spectra for $|t^{(0)}|^2$, $|r^{(0)}|^2$, $|t^{(\pm1)}|^2$, and $|r^{(\pm1)}|^2$, respectively, while changing the detuning of the input photon, Δ, and the Rabi frequency strength of the driving field, Ω. Δ is scanned from $-30V^2/v_g$ to $30V^2/v_g$, covering the two atomic resonances at ω_a ($\Delta = -5\ V^2/v_g$) and ω_b ($\Delta = 5V^2/v_g$). Ω is scanned from 0 to $25V^2/v_g$. At $\Omega = 0$, that is, the external driving field is turned off, the single-photon transport shows the complete reflection if the incident photon has the frequency at the resonances of ω_a and ω_b (see Figure 2b), while it results in the complete transmission if the photon is not near resonant with ω_a and ω_b (see Figure 2a). Without the driving field, the frequency of the transmitted/reflected photon can not be converted to other frequency component at $\omega_{n\neq0}$. Once the driving field is turned on, the frequency of the photon can be converted due to the photon−photon interaction between the waveguide photon and the photon from the driving field through the atom. For example, the incident photon at the frequency ω excites the atomic transition $|g\rangle \rightarrow |a\rangle$ first, the driving field then converts the atom from $|a\rangle \rightarrow |b\rangle$, and last a new photon is emitted from the transition $|b\rangle \rightarrow |g\rangle$, coupling back to the waveguide and propagating toward either the right or the left. The probability of this conversion path is captured by the transmission probability and reflection probability for photon at the frequency component ω_1, which are shown in Figure 2c. One can see the transmission/reflection probability becomes nonzero near the resonance at $\Delta = -\delta/2$ ($\omega = \omega_a$). On the other hand, another similar path showing the conversion to the frequency component ω_{-1} is featured by Figure 2d, where the transmission/reflection probability becomes nonzero near the resonance at $\Delta = \delta/2$ ($\omega = \omega_b$). For small Ω of the driving field, the spectra in Figure 2 show the linear Rabi splitting near resonances, which is consistent with the results in ref 42. Nevertheless, features of the linear Rabi splitting is no longer valid for the strong driving breaking RWA between two excited states, that is, $\Omega \sim \delta/2$, because of the counter-rotating terms from the interaction between the driving field and the atom. By further increasing the Rabi frequency ($\Omega > \delta/2$), one can see the anticrossing features in the spectra near $\Delta = \pm 15V^2/v_g$ and $\Delta = \pm\ 25V^2/v_g$ in Figure 2, which corresponds to the resonance from the virtual photon transition from the counter-rotating terms. Other interesting features from the strong external driving between two excited states can be seen. For example, the spectra for converted-frequency photon in Figure 2c,d show the nonlinear dependence, indicating that the creation of the photon at $\omega_{\pm1}$ has local maximum for a certain parameter regime.

To better explore the conversion probability of the incident photon to different frequency components at ω_n, we set $\Delta = 0$ and plot the corresponding transmitted/reflected spectra $|t^{(n)}|^2$ and $|r^{(n)}|^2$ in Figure 3a,b, while varying Ω. It is interesting to see

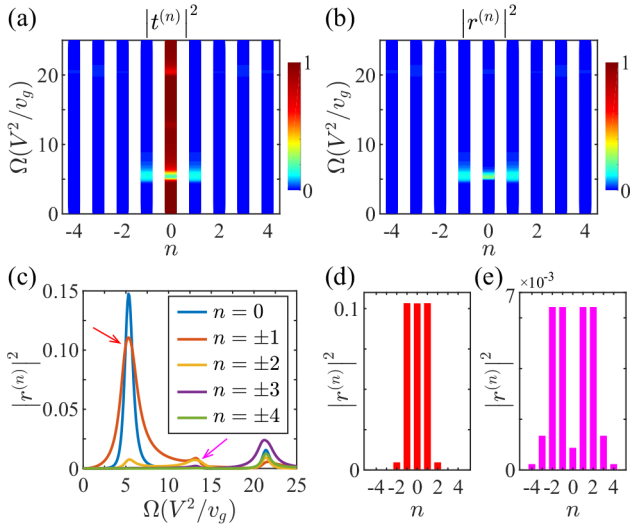

Figure 3. (a, b) Transmission and reflection coefficients ($|t^{(n)}|^2$ and $|r^{(n)}|^2$) for the incident photon having $\Delta = 0$. (c) The corresponding $|r^{(n)}|^2$ with $n = 0, \pm1, ..., \pm4$. (d, e) Spectra of the reflected output photon at $\Omega = 4.971V^2/v_g$ [labeled by red arrow in (c)] and $\Omega = 13.590V^2/v_g$ [labeled by magenta arrow in (c)], respectively.

symmetric spectra and to note that the probabilities for converted frequency components at $|n| \geq 2$ is almost zero. Moreover, at $\Omega \approx 5\ V^2/v_g$, reflected spectra shows similar amplitudes for components $n = 0, \pm1$, which indicates that, for the incident photon at the frequency $\omega = (\omega_a + \omega_b)/2$ interacting with the driven atom, it exhibits similar probabilities for the reflected photon converted to the frequency $\omega - \delta$, ω, or $\omega + \delta$. We further plot reflected

https://dx.doi.org/10.1021/acsphotonics.0c00263
ACS Photonics 2020, 7, 2010−2017

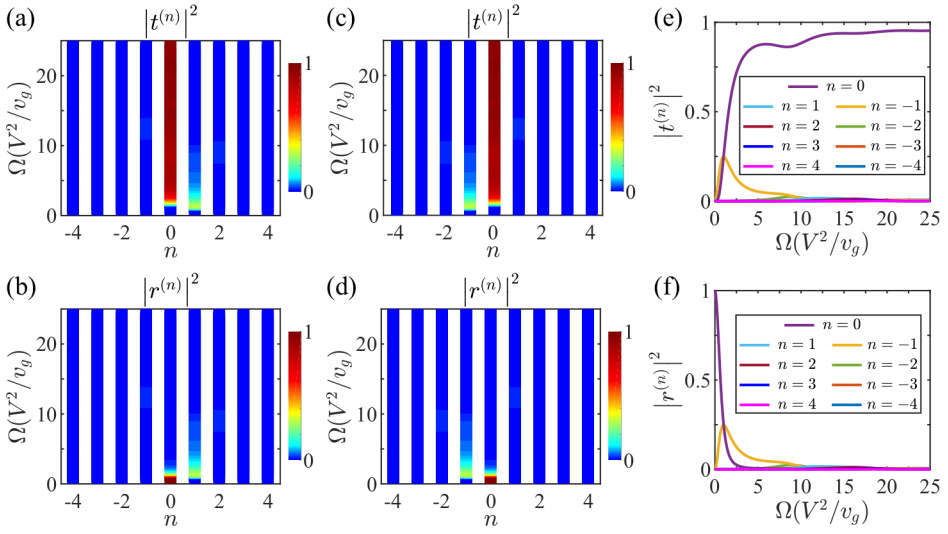

Figure 4. (a, b) [(c, d)] Transmission and reflection coefficients ($|t^{(n)}|^2$ and $|r^{(n)}|^2$) for the incident photon having $\Delta = -\delta/2$ ($\Delta = \delta/2$). (e, f) Corresponding $|t^{(n)}|^2$ and $|r^{(n)}|^2$ with $n = 0, \pm1, ..., \pm4$ for the incident photon having $\Delta = \delta/2$.

spectra $|r^{(n)}|^2$ versus Ω in Figure 3c. One can see that the reflection coefficients for $n = -1, 0, 1$ are the same at $\Omega = 4.971V^2/v_g$, with its corresponding reflected spectra detailed in Figure 3d. With this choice of the driving Rabi frequency, the probability for the reflected photon collected at the left having the frequency $\omega_{0,\pm1}$ is 0.104. This unique feature here can be used for generating a correlated single-photon state along the frequency axis of light

$$|\phi_{c1}\rangle = |1_{-1}, 0_0, 0_1\rangle + |0_{-1}, 1_0, 0_1\rangle + |0_{-1}, 0_0, 1_1\rangle \tag{12}$$

if the postselection is applied to filter out the photon transmitted to the right. Similar feature can also been found for $\Omega = 5.730V^2/v_g$. Moreover, one can use the spectra in Figure 3c to consider different correlated photon generation. For example, in Figure 3e, we plot the reflected spectra with $\Omega = 13.590V^2/v_g$, which shows the reflected photon has the equal probability to be converted to the frequency components at $\omega \pm \delta$ and $\omega \pm 2\delta$, respectively, while conversions to other frequency components are highly negligible, leading to the potential generation of the correlated single-photon state:

$$|\phi_{c2}\rangle = |1_{-2}, 0_{-1}, 0_1, 0_2\rangle + |0_{-2}, 1_{-1}, 0_1, 0_2\rangle + |0_{-2}, 0_{-1}, 1_1, 0_2\rangle + |0_{-2}, 0_{-1}, 0_1, 1_2\rangle \tag{13}$$

We next choose the frequency of the incident photon being $\omega = \omega_a$ ($\Delta = -\delta/2$) and $\omega = \omega_b$ ($\Delta = \delta/2$), respectively, which is equal to the two atomic resonances in Figure 1a. Figure 4a,b (Figure 4c,d) show transmitted/reflected spectra $|t^{(n)}|^2$ and $|r^{(n)}|^2$ for the case $\omega = \omega_a$ ($\omega = \omega_b$). Asymmetric spectra have been seen, which shows the unidirectional frequency conversions of the output photon. We plot the corresponding $|t^{(n)}|^2$ and $|r^{(n)}|^2$ versus Ω for the case of $\omega = \omega_b$ in Figure 4e,f. One notice that there are high possibilities of the photon remaining its original frequency or getting converted to the frequency ω_{-1}. Moreover, as shown in Figure 4f, $|r^{(0)}|^2$ starts from 1 and drops to 0, while Ω is increasing. Meanwhile, $|r^{(-1)}|^2$ starts from 0 to its maximum probability ~0.25 at $\Omega \approx 1.003V^2/v_g$, and it gradually drops to 0 while Ω is further increasing. We notice that near $\Omega = 4.393\ V^2/v_g$, $|r^{(0)}|^2 \approx 0$, but $|r^{(-1)}|^2 \approx 0.061$. Therefore, this feature can be used to convert the input photon at the frequency ω_b to a reflected photon at ω_a if the postselection is used to filter out the transmitted photon. Due to the symmetry between spectra in Figure 4a,b and Figure 4c,d, a photon at ω_a can also be converted to the photon at ω_b with the postselection.

To further see the quantum interferences between virtual transition paths, we also calculate the single-photon transport with the atom having $\delta = 5V^2/v_g$. In Figure 5a,b, we show the

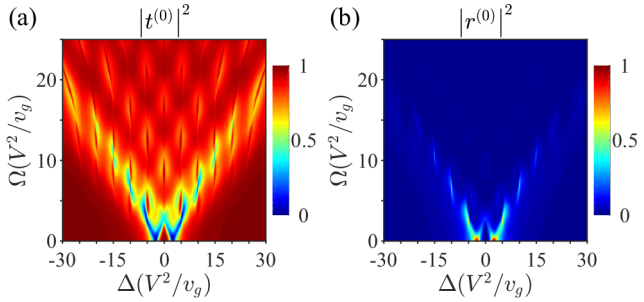

Figure 5. (a, b) Transmission and reflection spectra $|t^{(0)}|^2$ and $|r^{(0)}|^2$ of the single-photon transport in the atom−waveguide system with $\delta = 5V^2/v_g$.

transmission and reflection spectra for $|t^{(0)}|^2$ and $|r^{(0)}|^2$, respectively. Besides similar features in Figure 2a,b, one can see a more complex pattern including the Rabi splitting as well as the anticrossing features around $\Delta = \pm(m + 1/2)\delta$, with m being a positive integer.

SIMULATIONS

In this section, we perform simulations to show the possibilities for generating frequency correlated photon states and achieving the single-photon frequency conversion. Simulations are based on solving equations of motion from eqs 1 and 2, which read

$$\left(\frac{\partial}{\partial t} + v_g\frac{\partial}{\partial x}\right)\phi_R(x, t) = -i\omega\phi_R(x, t) - iV\delta(x)[e_1(t) + e_2(t)] \tag{14}$$

$$\left(\frac{\partial}{\partial t} - v_g\frac{\partial}{\partial x}\right)\phi_L(x, t) = -i\omega\phi_L(x, t) - iV\delta(x)[e_1(t) + e_2(t)] \tag{15}$$

https://dx.doi.org/10.1021/acsphotonics.0c00263
ACS Photonics 2020, 7, 2010−2017

$$\dot{e}_1(t) = -i\omega_a e_1(t) - iV\int dx\delta(x)[\phi_R(x,t) + \phi_L(x,t)] - i2\Omega\cos(\delta t)e_2(t) \quad (16)$$

$$\dot{e}_2(t) = -i\omega_b e_2(t) - iV\int dx\delta(x)[\phi_R(x,t) + \phi_L(x,t)] - i2\Omega\cos(\delta t)e_1(t) \quad (17)$$

In simulations, we use a Gaussian-shape pulse with the carrier frequency ω and the full width at half-maximum being $0.25V^2/v_g$ as the input field. We also set $\delta = 10V^2/v_g$. The input field is injected from the left of the waveguide propagating toward the right. We collect the temporal profiles of the right-propagating field at the right end and the left-propagating field at the left end of the waveguide, and then perform the Fourier transformation to show the transmission and reflection spectra, respectively.

We first show simulation results of the case with the input carrier frequency being $\omega = \omega_a + \delta/2$, which correspond to the proposed generation of the correlated single-photon state in Figure 3d,e. Figure 6a and b show the output transmission and reflection spectra with $\Omega = 4.971V^2/v_g$ and $13.590V^2/v_g$, respectively. In Figure 6a, one can see that the output spectrum for the reflected field indeed gives three major peaks at frequencies $\omega_a + \delta/2 - \delta$, $\omega_a + \delta/2$, $\omega_a + \delta/2 + \delta$, respectively, with almost equally intensities. This feature is consistent with the analysis in Figure 3d. In Figure 6b, there are four major peaks at frequencies $\omega_a + \delta/2 - 2\delta$, $\omega_a + \delta/2 - \delta$, $\omega_a + \delta/2 + \delta$, $\omega_a + \delta/2 + 2\delta$ in the reflected spectrum. We find it quantitatively matches what we expected to see from Figure 3e, however, the intensities of these four peaks are not at the same intensity. The reason is that such small amount of reflection is difficult to be accurately captured from a finite temporal pulse that we use in simulations. The transmission spectrum shows a single peak at the input frequency dominating other frequency components, which indicates that the photon has a very large chance to be transparency through the waveguide in this untrastrong driving case.

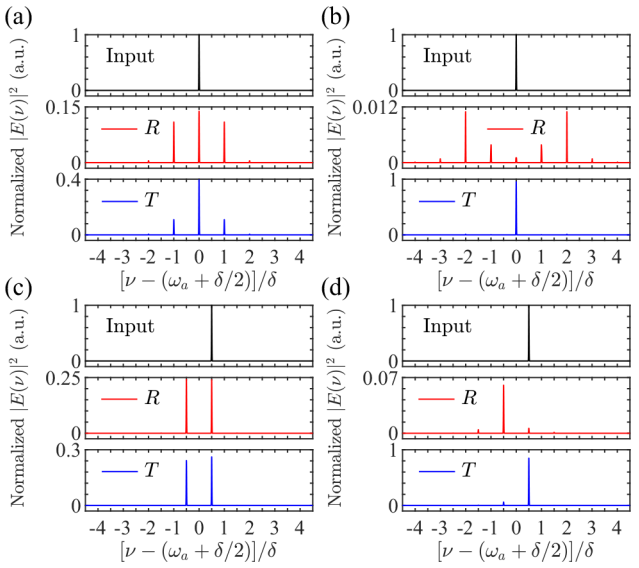

Figure 6. (a, b) The input (black), output reflection (red), and output transmission (blue) spectra for incident photon $\Delta = 0$, with $\Omega = 4.971\ V^2/v_g$ and $13.590V^2/v_g$, respectively. (c, d) The input (black), output reflection (red), and output transmission (blue) spectra for incident photon $\Delta = 5V^2/v_g$ with $\Omega = 1.003V^2/v_g$ and $4.393V^2/v_g$, respectively. Here $\delta = 10V^2/v_g$.

We then change the input photon at the carrier frequency $\omega = \omega_b = \omega_a + \delta$, but keep the atom and the waveguide system unchanged. We use the drive field at different strengths and Figure 6c and d gives the simulation results with $\Omega = 1.003V^2/v_g$ and $4.393V^2/v_g$, respectively. In Figure 6c, one can see the output spectra for both the transmission and the reflection show two equally distributed peaks at frequencies ω_a and ω_b, which are consistent with the analysis of Figure 4e,f. One can then use this frequency conversion result to prepare a correlated state based on these two frequencies. Moreover, Figure 6d shows the complete unidirectional frequency conversion in the reflection as the output reflected spectrum has a peak at ω_a, while the transmitted spectrum has the peak at ω_b. Therefore, simulations confirm the analysis in the previous section that one can generate the desired correlated photon state or perform the single-photon frequency conversion with the postselection by choosing appropriate external drive field in the same atom-waveguide system.

DISCUSSION AND SUMMARY

Our proposal can be potentially realized in different types of atom−light interaction systems.[3,12,57−61] In particular, it is experimentally demonstrated that a single microwave photon can interacting with a superconducting qubit in a waveguide resonator, with a resonant frequency at the order of 1−10 GHz and $V^2/v_g \approx 0.1$−1 MHz.[12,21] Such superconducting qubit is capable for being designed in V-type scheme with upper level splitting ≈1−10 MHz coherently driven by an external field at the Rabi frequency up to 10 MHz.[58,62] Alternatively, one could also consider to use the photonic atom−waveguide experimental platform.[3,59,61] In this case, one embeds either the rubidium or cesium atom into a photonic-crystal waveguide, where the coupling strength can be achieved at the order of ≈1−10^3 MHz.[3,59,61] To construct a V-type level scheme, the hyperfine splitting of one excited state of the atom can be used with the level splitting at the order of 0.1−1 GHz.[63,64] This hyperfine transition can be coupled by the coherent microwave field.[65] Moreover, our proposal is also potentially feasible in the phonon−atom coupling system.[60] With recent rapidly developing state-of-art technologies, we see various experimental possibilities for further on-chip implementations of our theoretical proposal.

There are few remarks we want to make here. In our driven atom−waveguide system in Figure 1, the waveguide photon can couple to both atomic transitions. In previous works regarding to waveguide photon interacting with multilevel atoms,[32,33,42,45,48,56,66,67] the assumption that the photon at certain frequency is only coupled to one of atomic transitions has been taken. This assumption is valid when the frequency difference between two atomic transitions is relatively large in a driven system. The linear splitting regime shown in spectra in Figures 2 and 5 is in this condition. On the other hand, the ultrastrong field is technologically available and practically important for achieving photon−photon interactions in nanophotonics.[5] However, for ultrastrong external drive, this assumption breaks and RWA is no longer valid. Our analysis hence explores this problem beyond RWA under the ultrastrong driving regime. Multifunctional single-photon manipulations along the frequency domain have been found. The resulting manipulation efficiencies are possible to be further improved with some extra efforts. For example, a

https://dx.doi.org/10.1021/acsphotonics.0c00263
ACS Photonics 2020, 7, 2010−2017

multistage coupling scheme where the single-photon transports in a 1D atomic chain and each atom is driven by an external field can be used. In this scheme, the frequency-conversion efficiency is estimated to be linearly increased with only few atoms added, and to approach the saturation ∼23% in a chain of ∼20 atoms, using the same parameters in Figure 6d. Moreover, efficiencies are possibly further increased by including an appropriate cavity into the system.

In summary, we study the single-photon transport in a waveguide, coupling with a three-level atom driven by the external field. Such an ultrastrong external field between two atomic excited states can induce an atomic virtual transtions. The single photon undergoes quantum interferences between different atomic transition paths and therefore spectra for the output photon exhibit anticrossing features. By changing the frequency of the input photon as well as the Rabi frequency of the driving field, one see the frequency conversion in the single-photon transport process, which could be important toward applications for the single-photon frequency modulator. Moreover, the reflected photon can also be used to generate different correlated single-photon states in the spectral domain. One notices that the Hamiltonian in eq 1 used to describe the atom−waveguide system in Figure 1a, can be similar to that describing a cavity−waveguide system with two cavities under a time-dependent coupling coefficient.[68,69] Hence, the phenomena in this work shall also be valid for such a system. Compared to previous works,[54,70−74] our proposal here provides an alternative method with flexibility in an atom-waveguide platform driven by tunable external driving field to achieve multiple functionalities, which is essential for the engineering purpose for manipulating single photon in integrated photonics.[3] Our work therefore shows the important spectral manipulation of the photon, which could bring new possibilities with the concept of synthetic dimensions,[75−78] including synthetic Fock-state lattices,[79−81] and point out the all-optical control of the photon, leading toward practical potentials in quantum information processing.[82−84]

AUTHOR INFORMATION

Corresponding Author

Luqi Yuan − *State Key Laboratory of Advanced Optical Communication Systems and Networks, School of Physics and Astronomy, Shanghai Jiao Tong University, Shanghai 200240, China;* orcid.org/0000-0001-9481-0247; Email: yuanluqi@sjtu.edu.cn

Authors

Han Xiao − *State Key Laboratory of Advanced Optical Communication Systems and Networks, School of Physics and Astronomy, Shanghai Jiao Tong University, Shanghai 200240, China*

Luojia Wang − *State Key Laboratory of Advanced Optical Communication Systems and Networks, School of Physics and Astronomy, Shanghai Jiao Tong University, Shanghai 200240, China*

Xianfeng Chen − *State Key Laboratory of Advanced Optical Communication Systems and Networks, School of Physics and Astronomy, Shanghai Jiao Tong University, Shanghai 200240, China; Collaborative Innovation Center of Light Manipulations and Applications, Shandong Normal University, Jinan 250358, China*

Complete contact information is available at: https://pubs.acs.org/10.1021/acsphotonics.0c00263

Author Contributions

[§]These authors contributed equally to this work.

Notes

The authors declare no competing financial interest.

ACKNOWLEDGMENTS

This paper is supported by National Natural Science Foundation of China (11974245), National Key R&D Program of China (2018YFA0306301 and 2017YFA0303701), and Natural Science Foundation of Shanghai (19ZR1475700).

REFERENCES

(1) Chen, W.; Beck, K. M.; Bücker, R.; Gullans, M.; Lukin, M. D.; Tanji-Suzuki, H.; Vuletić, V. All-Optical Switch and Transistor Gated by One Stored Photon. *Science* **2013**, *341*, 768−770.

(2) Gorniaczyk, H.; Tresp, C.; Schmidt, J.; Fedder, H.; Hofferberth, S. Single-Photon Transistor Mediated by Interstate Rydberg Interactions. *Phys. Rev. Lett.* **2014**, *113*, 053601.

(3) Goban, A.; Hung, C.-L.; Yu, S.-P.; Hood, J. D.; Muniz, J. A.; Lee, J. H.; Martin, M. J.; McClung, A. C.; Choi, K. S.; Chang, D. E.; Painter, O.; Kimble, H. J. Atom−light interactions in photonic crystals. *Nat. Commun.* **2014**, *5*, 3808.

(4) Shomroni, I.; Rosenblum, S.; Lovsky, Y.; Bechler, O.; Guendelman, G.; Dayan, B. All-optical routing of single photons by a one-atom switch controlled by a single photon. *Science* **2014**, *345*, 903−906.

(5) Chang, D. E.; Vuletić, V.; Lukin, M. D. Quantum nonlinear optics − photon by photon. *Nat. Photonics* **2014**, *8*, 685−694.

(6) Hacker, B.; Welte, S.; Rempe, G.; Ritter, S. A photon−photon quantum gate based on a single atom in an optical resonator. *Nature* **2016**, *536*, 193−196.

(7) Lodahl, P.; Mahmoodian, S.; Stobbe, S.; Rauschenbeutel, A.; Schneeweiss, P.; Volz, J.; Pichler, H.; Zoller, P. Chiral quantum optics. *Nature* **2017**, *541*, 473−480.

(8) Barik, S.; Karasahin, A.; Flower, C.; Cai, T.; Miyake, H.; DeGottardi, W.; Hafezi, M.; Waks, E. A topological quantum optics interface. *Science* **2018**, *359*, 666−668.

(9) Chang, D. E.; Douglas, J. S.; González-Tudela, A.; Hung, C.-L.; Kimble, H. J. Colloquium: Quantum matter built from nanoscopic lattices of atoms and photons. *Rev. Mod. Phys.* **2018**, *90*, 031002.

(10) Zhang, A.; Wang, L.; Chen, X.; Yakovlev, V. V.; Yuan, L. Tunable super- and subradiant boundary states in one-dimensional atomic arrays. *Commun. Phys.* **2019**, *2*, 157.

(11) Calajó, G.; Fang, Y. L.; Baranger, H. U.; Ciccarello, F. Exciting a Bound State in the Continuum through Multiphoton Scattering Plus Delayed Quantum Feedback. *Phys. Rev. Lett.* **2019**, *122*, 073601.

(12) Wallraff, A.; Schuster, D. I.; Blais, A.; Frunzio, L.; Huang, R.-S.; Majer, J.; Kumar, S.; Girvin, S. M.; Schoelkopf, R. J. Strong coupling of a single photon to a superconducting qubit using circuit quantum electrodynamics. *Nature* **2004**, *431*, 162−167.

(13) Houck, A. A.; Schuster, D. I.; Gambetta, J. M.; Schreier, J. A.; Johnson, B. R.; Chow, J. M.; Frunzio, L.; Majer, J.; Devoret, M. H.; Girvin, S. M.; Schoelkopf, R. J. Generating single microwave photons in a circuit. *Nature* **2007**, *449*, 328−331.

(14) Chang, D. E.; Sørensen, A. S.; Demler, E. A.; Lukin, M. D. A single-photon transistor using nanoscale surface plasmons. *Nat. Phys.* **2007**, *3*, 807−812.

(15) Petersen, J.; Volz, J.; Rauschenbeutel, A. Chiral nanophotonic waveguide interface based on spin-orbit interaction of light. *Science* **2014**, *346*, 67−71.

(16) Mitsch, R.; Sayrin, C.; Albrecht, B.; Schneeweiss, P.; Rauschenbeutel, A. Quantum state-controlled directional spontaneous emission of photons into a nanophotonic waveguide. *Nat. Commun.* **2014**, *5*, 5713.

(17) Javadi, A.; Söllner, I.; Arcari, M.; Hansen, S. L.; Midolo, L.; Mahmoodian, S.; Kiršanskė, G.; Pregnolato, T.; Lee, E. H.; Song, J. D.; Stobbe, S.; Lodahl, P. Single-photon non-linear optics with a quantum dot in a waveguide. *Nat. Commun.* **2015**, *6*, 8655.
(18) Söllner, I.; Mahmoodian, S.; Hansen, S. L.; Midolo, L.; Javadi, A.; Kiršanskė, G.; Pregnolato, T.; El-Ella, H.; Lee, E. H.; Song, J. D.; Stobbe, S.; Lodahl, P. Deterministic photon−emitter coupling in chiral photonic circuits. *Nat. Nanotechnol.* **2015**, *10*, 775−778.
(19) Sayrin, C.; Junge, C.; Mitsch, R.; Albrecht, B.; O'Shea, D.; Schneeweiss, P.; Volz, J.; Rauschenbeutel, A. Nanophotonic Optical Isolator Controlled by the Internal State of Cold Atoms. *Phys. Rev. X* **2015**, *5*, 041036.
(20) Coles, R. J.; Price, D. M.; Dixon, J. E.; Royall, B.; Clarke, E.; Kok, P.; Skolnick, M. S.; Fox, A. M.; Makhonin, M. N. Chirality of nanophotonic waveguide with embedded quantum emitter for unidirectional spin transfer. *Nat. Commun.* **2016**, *7*, 11183.
(21) Shen, J.-T.; Fan, S. Coherent Single Photon Transport in a One-Dimensional Waveguide Coupled with Superconducting Quantum Bits. *Phys. Rev. Lett.* **2005**, *95*, 213001.
(22) Shen, J.-T.; Fan, S. Theory of single-photon transport in a single-mode waveguide. I. Coupling to a cavity containing a two-level atom. *Phys. Rev. A: At., Mol., Opt. Phys.* **2009**, *79*, 023837.
(23) Ciuti, C.; Carusotto, I. Input-output theory of cavities in the ultrastrong coupling regime: The case of time-independent cavity parameters. *Phys. Rev. A: At., Mol., Opt. Phys.* **2006**, *74*, 033811.
(24) Fan, S.; Kocabas, Ş. E.; Shen, J.-T. Input-output formalism for few-photon transport in one-dimensional nanophotonic waveguides coupled to a qubit. *Phys. Rev. A: At., Mol., Opt. Phys.* **2010**, *82*, 063821.
(25) Roy, D. Two-Photon Scattering by a Driven Three-Level Emitter in a One-Dimensional Waveguide and Electromagnetically Induced Transparency. *Phys. Rev. Lett.* **2011**, *106*, 053601.
(26) Le Kien, F.; Rauschenbeutel, A. Electromagnetically induced transparency for guided light in an atomic array outside an optical nanofiber. *Phys. Rev. A: At., Mol., Opt. Phys.* **2015**, *91*, 053847.
(27) Sánchez-Burillo, E.; Martín-Moreno, L.; Zueco, D.; García-Ripoll, J. J. One- and two-photon scattering from generalized V-type atoms. *Phys. Rev. A: At., Mol., Opt. Phys.* **2016**, *94*, 053857.
(28) Zang, X.; Zhou, T.; Cai, B.; Zhu, Y. Single-photon transport properties in an optical waveguide coupled with a Λ-type three-level atom. *J. Opt. Soc. Am. B* **2013**, *30*, 1135−1140.
(29) Rephaeli, E.; Fan, S. Stimulated Emission from a Single Excited Atom in a Waveguide. *Phys. Rev. Lett.* **2012**, *108*, 143602.
(30) Liao, J.-Q.; Law, C. K. Correlated two-photon transport in a one-dimensional waveguide side-coupled to a nonlinear cavity. *Phys. Rev. A: At., Mol., Opt. Phys.* **2010**, *82*, 053836.
(31) Zheng, H.; Gauthier, D. J.; Baranger, H. U. Strongly correlated photons generated by coupling a three- or four-level system to a waveguide. *Phys. Rev. A: At., Mol., Opt. Phys.* **2012**, *85*, 043832.
(32) Zheng, H.; Gauthier, D. J.; Baranger, H. U. Waveguide-QED-Based Photonic Quantum Computation. *Phys. Rev. Lett.* **2013**, *111*, 090502.
(33) Wang, Z. H.; Zhou, L.; Li, Y.; Sun, C. P. Controllable single-photon frequency converter via a one-dimensional waveguide. *Phys. Rev. A: At., Mol., Opt. Phys.* **2014**, *89*, 053813.
(34) Xu, S.; Fan, S. Input-output formalism for few-photon transport: A systematic treatment beyond two photons. *Phys. Rev. A: At., Mol., Opt. Phys.* **2015**, *91*, 043845.
(35) Özgün, E.; Ozbay, E.; Caglayan, H. Tunable Zero-Index Photonic Crystal Waveguide for Two-Qubit Entanglement Detection. *ACS Photonics* **2016**, *3*, 2129−2133.
(36) Liao, Z.; Nha, H.; Zubairy, M. S. Single-photon frequency-comb generation in a one-dimensional waveguide coupled to two atomic arrays. *Phys. Rev. A: At., Mol., Opt. Phys.* **2016**, *93*, 033851.
(37) Zhou, M.; Liu, J.; Kats, M. A.; Yu, Z. Optical Metasurface Based on the Resonant Scattering in Electronic Transitions. *ACS Photonics* **2017**, *4*, 1279−1285.
(38) Zhou, Y.; Chen, Z.; Shen, J.-T. Single-photon superradiant emission rate scaling for atoms trapped in a photonic waveguide. *Phys. Rev. A: At., Mol., Opt. Phys.* **2017**, *95*, 043832.
(39) Chen, G.-Y.; Lambert, N.; Shih, Y.-A.; Liu, M.-H.; Chen, Y.-N.; Nori, F. Plasmonic bio-sensing for the Fenna−Matthews−Olson complex. *Sci. Rep.* **2017**, *7*, 39720.
(40) Trivedi, R.; Fischer, K.; Xu, S.; Fan, S.; Vuckovic, J. Few-photon scattering and emission from low-dimensional quantum systems. *Phys. Rev. B: Condens. Matter Mater. Phys.* **2018**, *98*, 144112.
(41) Zhou, Y.; Chen, Z.; Wang, L. V.; Shen, J.-T. Efficient two-photon excitation by photonic dimers. *Opt. Lett.* **2019**, *44*, 475−478.
(42) Yuan, L.; Xu, S.; Fan, S. Achieving nonreciprocal unidirectional single-photon quantum transport using the photonic Aharonov−Bohm effect. *Opt. Lett.* **2015**, *40*, 5140−5143.
(43) Gonzalez-Ballestero, C.; Moreno, E.; Garcia-Vidal, F. J.; Gonzalez-Tudela, A. Nonreciprocal few-photon routing schemes based on chiral waveguide-emitter couplings. *Phys. Rev. A: At., Mol., Opt. Phys.* **2016**, *94*, 063817.
(44) Cheng, M.-T.; Ma, X.; Fan, J.-W.; Xu, J.; Zhu, C. Controllable single-photon nonreciprocal propagation between two waveguides chirally coupled to a quantum emitter. *Opt. Lett.* **2017**, *42*, 2914−2917.
(45) Yan, C.-H.; Li, Y.; Yuan, H.; Wei, L. F. Targeted photonic routers with chiral photon-atom interactions. *Phys. Rev. A: At., Mol., Opt. Phys.* **2018**, *97*, 023821.
(46) Mirza, I. M.; Ge, W.; Jing, H. Optical nonreciprocity and slow light in coupled spinning optomechanical resonators. *Opt. Express* **2019**, *27*, 25515−25530.
(47) Tiecke, T. G.; Thompson, J. D.; de Leon, N. P.; Liu, L. R.; Vuletić, V.; Lukin, M. D. Nanophotonic quantum phase switch with a single atom. *Nature* **2014**, *508*, 241−244.
(48) Zhou, L.; Yang, L.-P.; Li, Y.; Sun, C. P. Quantum Routing of Single Photons with a Cyclic Three-Level System. *Phys. Rev. Lett.* **2013**, *111*, 103604.
(49) Yang, D.-C.; Cheng, M.-T.; Ma, X.-S.; Xu, J.; Zhu, C.; Huang, X.-S. Phase-modulated single-photon router. *Phys. Rev. A: At., Mol., Opt. Phys.* **2018**, *98*, 063809.
(50) Ramelow, S.; Ratschbacher, L.; Fedrizzi, A.; Langford, N. K.; Zeilinger, A. Discrete Tunable Color Entanglement. *Phys. Rev. Lett.* **2009**, *103*, 253601.
(51) Zavatta, A.; Artoni, M.; Viscor, D.; La Rocca, G. Manipulating Frequency-bin Entangled States in Cold Atoms. *Sci. Rep.* **2015**, *4*, 3941.
(52) Shirley, J. H. Solution of the Schrödinger Equation with a Hamiltonian Periodic in Time. *Phys. Rev.* **1965**, *138*, B979−B987.
(53) Sambe, H. Steady States and Quasienergies of a Quantum-Mechanical System in an Oscillating Field. *Phys. Rev. A: At., Mol., Opt. Phys.* **1973**, *7*, 2203.
(54) Wagner, M.; Vasilopoulos, P. Dynamics of strongly driven two-level systems: analytical solutions. *Superlattices Microstruct.* **1998**, *23*, 477−483.
(55) Fearn, H.; Scully, M. O.; Zhu, S. Y.; Sargent, M., III Lasing without inversion III: microwave coupling induced atomic coherence. *Z. Phys. D: At., Mol. Clusters* **1992**, *22*, 495−509.
(56) Yuan, L.; Hokr, B. H.; Traverso, A. J.; Voronine, D. V.; Rostovtsev, Y.; Sokolov, A. V.; Scully, M. O. Theoretical analysis of the coherence-brightened laser in air. *Phys. Rev. A: At., Mol., Opt. Phys.* **2013**, *87*, 023826.
(57) You, J. Q.; Nori, F. Atomic physics and quantum optics using superconducting circuits. *Nature* **2011**, *474*, 589−597.
(58) van Loo, A. F.; Fedorov, A.; Lalumière, K.; Sanders, B. C.; Blais, A.; Wallraff, A. Photon-Mediated Interactions Between Distant Artificial Atoms. *Science* **2013**, *342*, 1494−1496.
(59) Yu, S.-P.; Hood, J. D.; Muniz, J. A.; Martin, M. J.; Norte, R.; Hung, C.-L.; Meenehan, S. M.; Cohen, J. D.; Painter, O.; Kimble, H. J. Nanowire photonic crystal waveguides for single-atom trapping and strong light-matter interactions. *Appl. Phys. Lett.* **2014**, *104*, 111103.

https://dx.doi.org/10.1021/acsphotonics.0c00263
ACS Photonics 2020, 7, 2010−2017

(60) Gustafsson, M. V.; Aref, T.; Kockum, A. F.; Ekström, M. K.; Johansson, G.; Delsing, P. Propagating phonons coupled to an artificial atom. *Science* **2014**, *346*, 207−211.
(61) González-Tudela, A.; Hung, C.-L.; Chang, D. E.; Cirac, J. I.; Kimble, H. J. Subwavelength vacuum lattices and atom−atom interactions in two-dimensional photonic crystals. *Nat. Photonics* **2015**, *9*, 320−325.
(62) Ren, W.; Liu, W.; Song, C.; Li, H.; Guo, Q.; Wang, Z.; Zheng, D.; Agarwal, G. S.; Scully, M. O.; Zhu, S.-Y.; Wang, H.; Wang, D.-W. Simultaneous excitation of two noninteracting atoms with time-frequency correlated photon pairs in a superconducting circuit. *arXiv:2004.07531* **2020**, na.
(63) Tai, C.; Happer, W.; Gupta, R. Hyperfine structure and lifetime measurements of the second-excited *D* states of rubidium and cesium by cascade fluorescence spectroscopy. *Phys. Rev. A: At., Mol., Opt. Phys.* **1975**, *12*, 736.
(64) Rafac, R. J.; Tanner, C. E. Measurement of the ^{133}Cs $6p\ ^2P_{1/2}$ state hyperfine structure. *Phys. Rev. A: At., Mol., Opt. Phys.* **1997**, *56*, 1027.
(65) Li, H.; Sautenkov, V. A.; Rostovtsev, Y. V.; Welch, G. R.; Hemmer, P. R.; Scully, M. O. Electromagnetically induced transparency controlled by a microwave field. *Phys. Rev. A: At., Mol., Opt. Phys.* **2009**, *80*, 023820.
(66) Wang, Z. H.; Sun, C. P.; Li, Y. Microwave degenerate parametric down-conversion with a single cyclic three-level system in a circuit-QED setups. *Phys. Rev. A: At., Mol., Opt. Phys.* **2015**, *91*, 043801.
(67) Jia, W. Z.; Wang, Y. W.; Liu, Y.-X. Efficient single-photon frequency conversion in the microwave domain using superconducting quantum circuits. *Phys. Rev. A: At., Mol., Opt. Phys.* **2017**, *96*, 053832.
(68) Fang, K.; Yu, Z.; Fan, S. Photonic Aharonov-Bohm Effect Based on Dynamic Modulation. *Phys. Rev. Lett.* **2012**, *108*, 153901.
(69) Fang, K.; Yu, Z.; Fan, S. Realizing effective magnetic field for photons by controlling the phase of dynamic modulation. *Nat. Photonics* **2012**, *6*, 782−787.
(70) Zhou, L.; Lu, J.; Sun, C. P. Coherent control of photon transmission: Slowing light in a coupled resonator waveguide doped with Λ atoms. *Phys. Rev. A: At., Mol., Opt. Phys.* **2007**, *76*, 012313.
(71) Tsoi, T. S.; Law, C. K. Single-photon scattering on Λ-type three-level atoms in a one-dimensional waveguide. *Phys. Rev. A: At., Mol., Opt. Phys.* **2009**, *80*, 033823.
(72) Bradford, M.; Shen, J.-T. Single-photon frequency conversion by exploiting quantum interference. *Phys. Rev. A: At., Mol., Opt. Phys.* **2012**, *85*, 043814.
(73) Bradford, M.; Obi, K. C.; Shen, J.-T. Efficient Single-Photon Frequency Conversion Using a Sagnac Interferometer. *Phys. Rev. Lett.* **2012**, *108*, 103902.
(74) Jia, W. Z.; Wang, Z. D. Single-photon transport in a one-dimensional waveguide coupling to a hybrid atom-optomechanical system. *Phys. Rev. A: At., Mol., Opt. Phys.* **2013**, *88*, 063821.
(75) Yuan, L.; Lin, Q.; Xiao, M.; Fan, S. Synthetic dimension in photonics. *Optica* **2018**, *5*, 1396−1405.
(76) Ozawa, T.; Price, H. M. Topological quantum matter in synthetic dimensions. *Nat. Rev. Phys.* **2019**, *1*, 349−357.
(77) Lustig, E.; Weimann, S.; Plotnik, Y.; Lumer, Y.; Bandres, M. A.; Szameit, A.; Segev, M. Photonic topological insulator in synthetic dimensions. *Nature* **2019**, *567*, 356−360.
(78) Dutt, A.; Lin, Q.; Yuan, L.; Minkov, M.; Xiao, M.; Fan, S. A single photonic cavity with two independent physical synthetic dimensions. *Science* **2020**, *367*, 59−64.
(79) Wang, D.-W.; Liu, R.-B.; Zhu, S.-Y.; Scully, M. O. Superradiance Lattice. *Phys. Rev. Lett.* **2015**, *114*, 043602.
(80) Wang, D.-W.; Cai, H.; Liu, R.-B.; Scully, M. O. Mesoscopic Superposition States Generated by Synthetic Spin-Orbit Interaction in Fock-State Lattices. *Phys. Rev. Lett.* **2016**, *116*, 220502.
(81) Cai, H.; Liu, J.; Wu, J.; He, Y.; Zhu, S.-Y.; Zhang, J.-X.; Wang, D.-W. Experimental Observation of Momentum-Space Chiral Edge Currents in Room-Temperature Atoms. *Phys. Rev. Lett.* **2019**, *122*, 023601.
(82) Hammerer, K.; Sørensen, A. S.; Polzik, E. S. Quantum interface between light and atomic ensembles. *Rev. Mod. Phys.* **2010**, *82*, 1041.
(83) Kok, P.; Lovett, B. W. *Introduction to Optical Quantum Information Processing*; Cambridge University Press, 2010.
(84) Migdall, A.; Polyakov, S. V.; Fan, J.; Bienfang, J. C. *Single-Photon Generation and Detection: Physics and Applications*; Academic Press, 2013.

https://dx.doi.org/10.1021/acsphotonics.0c00263
ACS Photonics 2020, 7, 2010−2017